

Weak measurement-based protocol for ergotropy protection in open quantum batteries

André H. A. Malavazi^{1,*}, Rishav Sagar^{1,†}, Borhan Ahmadi^{1,‡} and Pedro R. Dieguez^{1,§}

¹*International Centre for Theory of Quantum Technologies,
University of Gdańsk, Jana Bażyńskiego 1A, 80-309 Gdańsk, Poland*

(Dated: November 26, 2024)

Quantum batteries are emerging as highly efficient energy storage devices that can exceed classical performance limits. Although there have been significant advancements in controlling these systems, challenges remain in stabilizing stored energy and minimizing losses due to inevitable environmental interaction. In this paper, we propose a protocol that employs selective weak measurements to protect quantum states from such influence and mitigate battery discharging. We establish thermodynamic constraints that allow this method to be implemented without disrupting the overall energy and ergotropy balance of the system. Our findings demonstrate that appropriately chosen measurement intensity can reduce unwanted discharging effects, thereby preserving ergotropy and improving the stability of quantum batteries. Additionally, we explore how weak measurements influence the coherent and incoherent components of ergotropy, providing new insights into the practical application of quantum coherence in energy storage technologies.

I. INTRODUCTION

In recent years, quantum batteries have emerged as promising devices for energy storage. These systems, composed of quantum states as energy carriers, aim to employ genuine quantum properties, such as coherence and entanglement, to surpass classical limits [1–6]. In this sense, quantum batteries were shown to exhibit unique features such as coherence-driven enhancements in ergotropy and charging processes [2, 6–8]. Significant progress has been made in understanding and manipulating these devices, with studies exploring diverse approaches like collisional models [9, 10], super- and sub-radiance [11], reservoir engineering [12, 13], phase transitions [14], micro-maser quantum batteries [15, 16], topological features [17, 18], catalysis [19], non-Markovian effects [20], optimal control strategies [21–23], and charging by measurement [24].

Various physical platforms have been proposed as viable candidates for quantum energy storage. Under cryogenic conditions, technologies such as superconducting circuits [23, 25–27], semiconductor quantum dots [28], ultracold-atoms [29], and nitrogen-vacancy centers in diamond [30] provide promising options, enabling quantum coherence and collective behavior necessary for efficient charging. On the other hand, room-temperature approaches, including organic micro-cavities [5] and nuclear spin systems [31, 32], showcase the potential for robust quantum energy storage through mechanisms that minimize decoherence, marking key advancements toward practical quantum batteries across a range of operating conditions.

Nevertheless, despite ongoing efforts, significant challenges persist, particularly in more realistic scenarios

where quantum coherence is susceptible to decoherence effects [33–43]. In this context, a charged quantum battery exposed to a dissipative environment renders not only the irreversible leakage of energy from the battery into the environment but also the loss of its charge, commonly quantified by the ergotropy, i.e., the extractable work from a quantum state [44]. For instance, the contact with a thermal reservoir leads the battery to a Gibbs state, which is completely passive [45]. Such effects are particularly detrimental to the performance of quantum technologies, as they limit the ability to harness ergotropy for practical applications. Therefore, characterizing and mitigating the influence of thermal reservoirs is essential for the reliable operation of quantum devices in general [46–48]. As proposed by [49], a possible way to preserve a quantum system from decaying is given by the continuous observation of the quantum system by a sequence of frequent projective measurements (a feature of the Zeno effect [50]), which can hinder the discharging process, effectively freezing the energy stored in a quantum battery. However, this method may not be experimentally friendly due to the required frequent state observation.

Furthermore, measurements are also being incorporated in quantum thermodynamics, e.g., as additional strokes in thermal cycles, with measurement-powered engines exploiting the fact that the measurement action generally disturbs the observed system, thereby altering its internal energy [51–53]. By employing non-selective measurements, for instance, a single temperature heat engine without feedback control to extract work was introduced [51], and several other measurement-based protocols have been explored [54–79]. In particular, since generalized measurements can be implemented as a sequence of weak measurements [80, 81], their intensity can be continuously adjusted to transition between weak and strong measurement regimes [82, 83]. Thus, weakly measured systems were shown to be crucial for consistently observing work and heat contributions in an externally driven quantum stochastic evolution [84] and were

* andrehamalavazi@gmail.com

† rishav.sagar@phdstud.ug.edu.pl

‡ borhan.ahmadi@ug.edu.pl

§ dieguez.pr@gmail.com

employed to develop a deterministic protocol based on non-selective variable strength measurements to perform a heat engine cycle [65, 78, 85]. Moreover, considering a bipartite correlated quantum system, selective weak measurements can offer more work extraction than the one described by the daemonic ergotropy [86], i.e., the amount of extractable work that arises from information gained in a strong (projective) measurement [87].

Here, we investigate the potentiality of weak measurements in attenuating environment-induced losses, aiming to harness quantum mechanical subtleties for more efficient energy storage and extraction in two-level systems-based quantum batteries. The protocol builds on the structure of previous theoretical and experimental studies on protecting quantum states from decoherence using weak measurements and measurement reversal operations [88–95]. The key distinction lies in our incorporation of thermodynamic-based constraints, enabling these methods to be applied without altering the overall energetics of the protocol. Specifically, before the discharging process, an initial weak measurement is performed, modifying the system energy and ergotropy. Subsequently, the charged system undergoes dissipative dynamics, during which a second weak measurement is carried out to compensate for the previously induced energetic and ergotropic changes. Despite the net exchange of these quantities being null, a positive gain can be observed at the end of the protocol. The feasibility of such a procedure is a direct consequence of the symmetry of the weak measurement and its reversal. Notably, without affecting the protocol’s overall probability of success, quantum coherence can be employed to enhance the measurement-based battery recovery process from discharging effects, as demonstrated in this work.

The remainder of this article is structured as follows. In Sec. II we introduce the physical context and model to explain the dissipation loss mitigation protocol. In Sec. III we present our main results by analyzing the protocol performance for the incoherent and coherent part of the ergotropy, as well as the total ergotropy, and identify parameter regions where the protocol yields promising outcomes. Finally, in Sec. IV, we summarize our main conclusions and discuss potential perspectives for future work.

II. ERGOTROPY LOSS MITIGATION PROTOCOL

Consider a d -dimensional quantum battery represented by the density matrix $\hat{\rho} = \sum_j^d p_j |j\rangle\langle j|$ and governed by the Hamiltonian $\hat{H} = \sum_k^d E_k |E_k\rangle\langle E_k|$. We assume that the probability distribution and energy spectrum are ordered as $p_1 > p_2 > \dots > p_d$ and $E_1 < E_2 < \dots < E_d$, respectively. The maximum amount of energy extractable via a unitary process that preserves cyclic Hamiltonian

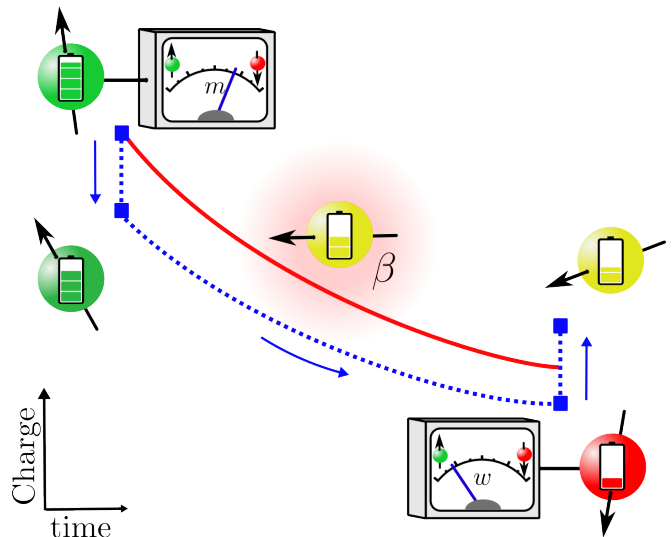


FIG. 1: **Ergotropy-protecting protocol based on weak measurements:** We consider a qubit quantum battery initially charged, which then undergoes a discharging process. Before this, a weak measurement with strength m is applied in the first step, changing the system’s ergotropy (charge) and energy (dashed blue line). In the intermediate step, during the discharging phase, a second reversal weak measurement with strength w is performed, compensating for the previous changes. Despite that, by carefully tuning the measurement intensities, the protocol can offer an advantage over a purely discharging process (continuous red line).

control is known as ergotropy, which is defined as [44]

$$\mathcal{R}[\hat{\rho}] := \text{Tr} \left[(\hat{\rho} - \hat{\rho}_p) \hat{H} \right] = \sum_{k,j}^d E_k p_j (|\langle E_k | j \rangle|^2 - \delta_{k,j}), \quad (1)$$

where $\hat{\rho}_p = \sum_i^d p_i |E_i\rangle\langle E_i|$ is the passive state, which is unitarily related to the initial state $\hat{\rho}$. Generally, the battery state may exhibit coherences in the \hat{H} basis, which is a unique quantum resource [96]. Identifying the contribution of coherence to the battery ergotropy is therefore insightful. To capture this, the coherent ergotropy within $\hat{\rho}$ is defined as [97–99]

$$\mathcal{R}^{coh}[\hat{\rho}] := \mathcal{R}[\hat{\rho}] - \mathcal{R}^{inc}[\hat{\rho}], \quad (2)$$

where $\mathcal{R}^{inc}[\hat{\rho}]$ represents the incoherent component of the ergotropy, such that $\mathcal{R}^{inc}[\hat{\rho}] = \mathcal{R}[\hat{\rho}^{diag}]$, where $\hat{\rho}^{diag} = \sum_k^d \langle E_k | \hat{\rho} | E_k \rangle |E_k\rangle\langle E_k|$ denotes the diagonal (incoherent) state of $\hat{\rho}$, obtained by removing its off-diagonal elements. Note that, by definition, $\mathcal{R}^{coh}[\hat{\rho}]$ is zero for incoherent states.

A. Setup and protocol description

For closed system dynamics, the ergotropy is preserved. Since the populations $\{p_j\}$ remain invariant under unitary dynamics, $\mathcal{R}[\hat{\rho}]$ remains unchanged during the free evolution of the battery. In contrast, if the battery is an open quantum system interacting with an external environment [33], its dynamics are no longer unitary, typically resulting in irreversible behavior that can lead to dissipation and discharging. Therefore, it is crucial to develop strategies to either stabilize its ergotropy or mitigate its inevitable leakage. To achieve this, we propose a protocol, depicted in Fig. 1, based on weak measurements performed before and after the battery discharging process.

More specifically, we consider a quantum battery composed of a single qubit weakly coupled to a thermal reservoir with inverse temperature β . The state of the battery is represented by $\hat{\rho}$, and its Hamiltonian is given by $\hat{H} = E_g|g\rangle\langle g| + E_e|e\rangle\langle e|$, where $E_e - E_g = \omega$ defines the qubit energy gap, with $|g\rangle$ ($|e\rangle$) corresponding to the ground (excited) state. Without loss of generality, we assume $E_g = 0$ for the rest of the paper. Notice that the maximum possible ergotropy for this system is given by ω , characterized by the state $|e\rangle\langle e|$. The time evolution of $\hat{\rho}$ is governed by the GKLS master equation [33] ($\hbar = k_B = 1$):

$$\frac{d}{dt}\hat{\rho}(t) = -i[\hat{H}, \hat{\rho}(t)] + \mathcal{D}_\downarrow[\hat{\rho}(t)] + \mathcal{D}_\uparrow[\hat{\rho}(t)], \quad (3)$$

where the dissipative terms are given by

$$\begin{aligned} \mathcal{D}_\downarrow[\cdot] &= \gamma(1-f) \left(\hat{\sigma}_+ \cdot \hat{\sigma}_- - \frac{1}{2} \{ \hat{\sigma}_- \hat{\sigma}_+, \cdot \} \right), \\ \mathcal{D}_\uparrow[\cdot] &= \gamma f \left(\hat{\sigma}_- \cdot \hat{\sigma}_+ - \frac{1}{2} \{ \hat{\sigma}_+ \hat{\sigma}_-, \cdot \} \right), \end{aligned} \quad (4)$$

where γ denotes the decay rate, $\hat{\sigma}_\pm = \hat{\sigma}_\pm^\dagger = |e\rangle\langle g|$ are the jump operators, and the thermal population is defined as $f = e^{-\beta\omega}(1 + e^{-\beta\omega})^{-1} \in [0, 1/2)$. The characteristic timescale of this dynamics is $\tau_\gamma = \gamma^{-1}$. Due to the form of the dissipators, the dynamical fixed point of Eq. (3) is the thermal (Gibbs) state $\hat{\tau}_{\text{th}} = (1-f)|g\rangle\langle g| + f|e\rangle\langle e|$, determined by the reservoir temperature. Thus, regardless of the initial state, we have $\lim_{t \rightarrow \infty} \hat{\rho}(t) = \hat{\tau}_{\text{th}}$. This time evolution results in an inevitable decay of ergotropy $\mathcal{R}[\hat{\rho}(t)]$ to zero, indicating the discharging of the battery as thermalization proceeds. Further details can be found in Appendix A.

The proposed protocol for mitigating ergotropy loss consists of the following steps: (i) Assume the battery is initially charged, meaning it has been prepared in an active state, such that $\hat{\rho}_0 = (1-P_0)|g\rangle\langle g| + P_0|e\rangle\langle e| + (Q_0|g\rangle\langle e| + h.c.)$, where $|Q_0|^2 \leq P_0(1-P_0)$ and $h.c.$ denotes the Hermitian conjugate; (ii) Immediately after charging, a weak measurement is performed of the form $\hat{M}_m := |g\rangle\langle g| + \sqrt{1-m}|e\rangle\langle e|$, with measurement strength

$0 \leq m \leq 1$. This process results in the post-measurement state

$$\hat{\rho}_m(0) = \frac{\hat{M}_m \hat{\rho}_0 \hat{M}_m^\dagger}{N_m}, \quad (5)$$

with probability

$$N_m := \text{Tr}[\hat{M}_m \hat{\rho}_0 \hat{M}_m^\dagger] = 1 - mP_0. \quad (6)$$

Notice that $\rho_m(0) = \rho_0 \forall m$ for a fully charged battery, i.e., $P_0 = 1$ and $Q_0 = 0$. In this particular case, the action of \hat{M}_m has no effect. However, due to the non-unitary nature of thermalization dynamics, we can generally have $P_0 < 1$ and proceed with the protocol; (iii) During a dissipation time $t \in [0, \tau]$, the battery is assumed to interact with the external environment. In this interval, its dynamics are governed by Eq. (3). Consequently, the state of the battery evolves as

$$\hat{\rho}_m(t) = \begin{pmatrix} 1 - P_m(t) & Q_m(t) \\ Q_m^*(t) & P_m(t) \end{pmatrix}, \quad (7)$$

with

$$\begin{aligned} P_m(t) &= \frac{P(t) - m[(1-f)e^{-\gamma t} + f]P_0}{N_m}, \\ Q_m(t) &= \frac{\sqrt{1-m}}{N_m} Q(t), \end{aligned} \quad (8)$$

where $P(t) = (P_0 - f)e^{-\gamma t} + f$ and $Q(t) = Q_0 e^{-\frac{\gamma t}{2} + it\omega}$ are the population and coherence, respectively, when no measurement is performed (i.e., $m = 0$) (see Appendix A); (iv) Finally, at instant $t = \tau$, a reversal measurement $\hat{W}_w := \sqrt{1-w}|g\rangle\langle g| + |e\rangle\langle e|$, with strength $0 \leq w \leq 1$, is performed. The resulting final state is then

$$\hat{\rho}_{mw}(\tau) = \frac{\hat{W}_w \hat{\rho}_m(\tau) \hat{W}_w^\dagger}{N_{mw}(\tau)} = \begin{pmatrix} 1 - P_{mw}(\tau) & Q_{mw}(\tau) \\ Q_{mw}^*(\tau) & P_{mw}(\tau) \end{pmatrix}, \quad (9)$$

with probability

$$\begin{aligned} N_{mw}(\tau) &:= \text{Tr}[\hat{W}_w \hat{\rho}_m(\tau) \hat{W}_w^\dagger] = 1 - w + w \frac{P(\tau)}{N_m} \\ &\quad - w \frac{(1-N_m)}{N_m} [(1-f)e^{-\gamma\tau} + f], \end{aligned} \quad (10)$$

in which

$$\begin{aligned} P_{mw}(\tau) &= N_{mw}^{-1}(\tau) P_m(\tau), \\ Q_{mw}(\tau) &= N_{mw}^{-1}(\tau) \sqrt{(1-w)} Q_m(\tau). \end{aligned} \quad (11)$$

The probability of successfully performing the protocol is defined as the product of the probabilities relative to the desired measurement outcomes as

$$\Pi_{mw}(\tau) := N_m N_{mw}(\tau). \quad (12)$$

It is important to emphasize that the measurements are assumed to be instantaneous. Also, note that the diagonal states and probabilities at each step are independent

of the initial coherence Q_0 . This independence arises from the commutation relations $[\hat{M}_m, \hat{H}] = [\hat{W}_w, \hat{H}] = 0$ and from Eq. (3), implying that the population changes induced by the successive actions of \hat{M}_m , thermalization dynamics, and \hat{W}_w do not couple them with the off-diagonal elements. The opposite, however, does not hold; that is, the coherence is coupled with the population during the measurements.

As previously mentioned, the ergotropy can be decomposed into coherent and incoherent parts, allowing us to quantify the final ergotropy of the battery as $\mathcal{R}_{mw}(\tau) := \mathcal{R}[\hat{\rho}_{mw}(\tau)] = \mathcal{R}_{mw}^{coh}(\tau) + \mathcal{R}_{mw}^{inc}(\tau)$. For two-level systems simple analytical expressions for both components can be derived [97, 98]. The incoherent component of the final ergotropy can be expressed as

$$\mathcal{R}_{mw}^{inc}(\tau) = \omega(2P_{mw}(\tau) - 1)[1 - \Theta(w' - w)], \quad (13)$$

where $\Theta(x)$ is the Heaviside function, such that $\Theta(x) = 1$ if $x \geq 0$ and null otherwise, and

$$w' := \frac{(1 - 2P_m(\tau))N_m}{N_m + (1 - N_m)[(1 - f)e^{-\gamma\tau} + f] - P(\tau)} \quad (14)$$

is the threshold strength for obtaining a finite final incoherent ergotropy, i.e., one has to guarantee $w > w'$ to have an active post-reversal measurement diagonal state. Additionally, the coherent component can be written as

$$\mathcal{R}_{mw}^{coh}(\tau) = \frac{1}{2} \left(\psi_{mw}(\tau) - \sqrt{\psi_{mw}^2(\tau) - 4|Q_{mw}(\tau)|^2} \right), \quad (15)$$

where $\psi_{mw}(\tau) := \sqrt{2\mu[\hat{\rho}_{mw}(\tau)] - 1}$, with $\mu[\hat{\rho}] := \text{Tr}[\hat{\rho}^2]$ being the purity of the state $\hat{\rho}$.

After successfully applying the described sequence of steps, a higher ergotropy in the final state is expected, compared to the amount one would have obtained without executing the protocol. In this sense, to quantify the performance of the procedure, we define the *ergotropy gain* as

$$\bar{\mathcal{R}}_{mw}(\tau) := \mathcal{R}_{mw}(\tau) - \mathcal{R}[\hat{\rho}(\tau)], \quad (16)$$

with $\hat{\rho}(\tau)$ being the state subjected only through the purely dissipative dynamics given by Eq. (3). This quantity can be also decomposed into coherent and incoherent parts, i.e.,

$$\bar{\mathcal{R}}_{mw}(\tau) = \bar{\mathcal{R}}_{mw}^{coh}(\tau) + \bar{\mathcal{R}}_{mw}^{inc}(\tau), \quad (17)$$

where

$$\bar{\mathcal{R}}_{mw}^{coh(inc)}(\tau) := \mathcal{R}_{mw}^{coh(inc)}(\tau) - \mathcal{R}^{coh(inc)}[\hat{\rho}(\tau)]. \quad (18)$$

In such a way the role of the initial coherence Q_0 in the protocol performance is fully captured by $\bar{\mathcal{R}}_{mw}^{coh}(\tau)$, i.e.,

given an initial state $\hat{\rho}_0$, this term quantifies the effect of Q_0 relative to the incoherent state $\hat{\rho}_0^{diag}$.

B. Protocol working regime

Note that the weak measurement and its reversal generally disturb the battery state; specifically, the former brings the battery closer to the ground state, while the latter pushes it toward the excited state. As a result, these protocol steps inevitably induce energy changes, potentially charging (or discharging) the battery. We therefore define $\varepsilon_{mw}(\tau)$ as the energy shift of the battery due to the measurements as

$$\begin{aligned} \varepsilon_{mw}(\tau) &:= \Delta E_m + \Delta E_{mw}(\tau) \\ &= \omega \left[\left(\frac{1-m}{N_m} - 1 \right) P_0 + P_{mw}(\tau) - P_m(\tau) \right], \end{aligned} \quad (19)$$

where

$$\begin{aligned} \Delta E_m &:= \text{Tr} \left[\hat{H} (\hat{\rho}_m(0) - \hat{\rho}_0) \right], \\ \Delta E_{mw}(\tau) &:= \text{Tr} \left[\hat{H} (\hat{\rho}_{mw}(\tau) - \hat{\rho}_m(\tau)) \right]. \end{aligned} \quad (20)$$

It is worth highlighting that such quantity is independent of the initial coherence of the battery Q_0 . In fact, $\varepsilon_{mw}(\tau)$ can be defined and computed only in terms of the diagonal (incoherent) component of the states. These changes may also be accompanied by an ergotropy shift $\mathcal{W}_{mw}(\tau)$, such that

$$\mathcal{W}_{mw}(\tau) := \Delta \mathcal{R}_m + \Delta \mathcal{R}_{mw}(\tau), \quad (21)$$

where

$$\begin{aligned} \Delta \mathcal{R}_m &:= \mathcal{R}[\hat{\rho}_m(0)] - \mathcal{R}[\hat{\rho}_0], \\ \Delta \mathcal{R}_{mw}(\tau) &:= \mathcal{R}[\hat{\rho}_{mw}(\tau)] - \mathcal{R}[\hat{\rho}_m(\tau)]. \end{aligned} \quad (22)$$

Hence, to ensure that the protocol does not actively provide a net external resource to the battery and effectively (dis)charge it, one should specify the measurement strengths m , w , and the dissipation time τ such that

$$\varepsilon_{mw}(\tau) = 0, \quad \mathcal{W}_{mw}(\tau) = 0. \quad (23)$$

The simultaneous validation of both requirements restricts the parameter space to valid working regions for our proposed protocol. In particular, for fixed values of γ , f , P_0 , m , and τ , one can show that the reversal measurement strength \tilde{w} needed to restore the energy lost due to the weak measurement is given by

$$\tilde{w} = N_m \frac{1 - P_0 - N_m(1 - f) + e^{\gamma\tau} [N_m(P_m(\tau) + P_0 - 1 - f) + 1 - P_0]}{[N_m(P_m(\tau) + P_0 - 1) + 1 - P_0] [N_m(1 - f)(e^{\gamma\tau} - 1) + 1 - P_0]}, \quad (24)$$

which ensures null energetic shift, $\varepsilon_{m\tilde{w}}(\tau) = 0$. Also, one should restrain into physical regions, characterized by strengths satisfying $\tilde{w} \in [0, 1]$. Hence, given Eq. (24), one can also find the subspace with null ergotropic shift, satisfying $\mathcal{W}_{m\tilde{w}}(\tau) = 0$ (see Appendix B for further discussion).

Along these lines, it is instructive to consider the particular case of equal measurement strengths, such that $m = w = \eta \in [0, 1]$. In such a scenario, it is possible to show that Eq. (24) reduces to the following null energetic shift strength curves

$$\begin{cases} \eta_1 := 0, \\ \eta_2 := \frac{f - P_0}{(f - 1)P_0}, \\ \eta_3 := \frac{e^{\gamma\tau}(f + P_0 - 1) - f + P_0}{P_0(e^{\gamma\tau}(f + P_0 - 1) - f + 1)}, \end{cases} \quad (25)$$

where η_1 is analogous to the trivial case of no measurements. The η_2 -curve is constant for fixed values of f and initial population P_0 , and it corresponds to protocols such that

$$\hat{\rho}_{\eta_2}(0) = \hat{\tau}_{\text{th}} + f \sqrt{\frac{f - 1}{f(P_0 - 1)P_0}} \begin{pmatrix} 0 & Q_0 \\ Q_0^* & 0 \end{pmatrix} \quad (26)$$

and

$$\hat{\rho}_{\eta_2\eta_2}(\tau) = \hat{\rho}_0^{\text{diag}} + e^{-\frac{1}{2}\tau\gamma} \begin{pmatrix} 0 & Q_0 e^{i\omega\tau} \\ Q_0^* e^{-i\omega\tau} & 0 \end{pmatrix} \quad (27)$$

for the post-measurement states. Note that after applying \hat{M}_{η_2} , the battery diagonal state, $\hat{\rho}_{\eta_2}^{\text{diag}}(0)$, is thermal with the inverse of temperature β , which remains invariant under the dissipative dynamics described by Eq. (3) (see Appendix A). This implies that while coherence decreases, no energy is lost due to environmental interaction. Then, after the application of \hat{W}_{η_2} , the diagonal state returns to its initial form, $\hat{\rho}_0^{\text{diag}}$, regardless of the elapsed time. Thus, the energy shifts induced by both measurements satisfy $\Delta E_{\eta_2} = -\Delta E_{\eta_2\eta_2}(\tau) = \omega(f - P_0)$ for all τ , ensuring $\varepsilon_{\eta_2\eta_2}(\tau) = 0$. For incoherent states, where $Q_0 = 0$, this results in a cyclic transformation $\hat{\rho}_0 \rightarrow \hat{\tau}_{\text{th}} \rightarrow \hat{\rho}_0$, so that $\Delta \mathcal{R}_{\eta_2} = -\Delta \mathcal{R}_{\eta_2\eta_2}(\tau)$ and $\mathcal{W}_{\eta_2\eta_2}(\tau) = 0$. On the other hand, the η_3 -curve explicitly depends on the dissipation time τ , leading to a non-trivial interpretation. Nonetheless, one can show that along this curve, it holds that $\Delta E_{\eta_3} = -\Delta E_{\eta_3\eta_3}(\tau) = \omega(f - P_0 - e^{\gamma\tau}(f + P_0 - 1))$.

In short, a successful and suitable application of the described protocol is characterized both by (i) a positive ergotropy gain, $\overline{\mathcal{R}}_{mw}(\tau) > 0$, and (ii) zero energy and ergotropy shifts, $\varepsilon_{mw}(\tau) = 0$ and $\mathcal{W}_{mw}(\tau) = 0$. In the following, we present our main results, demonstrating that this protocol yields an ergotropy gain, effectively mitigating battery discharging when the two measurement intensities and dissipation time are appropriately selected.

Additionally, we identify the impact of both the coherent and incoherent components of the battery ergotropy. It will be assumed $\omega = 1$, $f = 0.3$ and $\gamma = 10^{-2}$ for the following analyzes.

III. ERGOTROPY GAIN: THE ROLE OF INCOHERENT AND COHERENT PARTS

A. Incoherent ergotropy

We begin our analysis by characterizing the protocol steps for the incoherent component of ergotropy, given by $\mathcal{R}^{\text{inc}}[\hat{\rho}] = \mathcal{R}[\hat{\rho}^{\text{diag}}]$. Note that, since the state populations are independent of the initial coherence at every step, this is equivalent to describing an incoherently prepared battery. Thus, for the initial state $\hat{\rho}_0$, the corresponding incoherent ergotropy can be written as

$$\mathcal{R}_i^{\text{inc}} = \omega(2P_0 - 1)[1 - \Theta(1/2 - P_0)], \quad (28)$$

where $P_0 > 1/2$ ensures that the state is active. During step (ii), the weak measurement slightly projects the battery toward the ground state, which inevitably decreases the battery ergotropy, i.e., $\mathcal{R}_{ii}^{\text{inc}} - \mathcal{R}_i^{\text{inc}} \leq 0$. Note that the post-weak measurement state $\hat{\rho}_m(0)$ will remain active as long as $m < 2 - P_0^{-1}$ is satisfied, meaning that if the measurement strength is high enough, the battery state will become passive. Consequently, the ergotropy can be expressed as

$$\mathcal{R}_{ii}^{\text{inc}} = \omega \left(1 - 2 \frac{1 - P_0}{N_m} \right) [1 - \Theta(m - 2 + P_0^{-1})]. \quad (29)$$

As previously mentioned, the unavoidable coupling with an external environment is detrimental to the stored ergotropy, which is asymptotically leaked, leading to $\mathcal{R}_{iii}^{\text{inc}} - \mathcal{R}_{ii}^{\text{inc}} \leq 0$ (see Appendix A for more details). During this process, the ergotropy is given by

$$\begin{aligned} \mathcal{R}_{iii}^{\text{inc}} &= 2\omega \left[\left(\frac{(1 - m)P_0}{N_m} - f \right) e^{-\gamma t} + f - \frac{1}{2} \right] \\ &\times [1 - \Theta(m - 2 + P_0^{-1})] [1 - \Theta(t - \tau_{1/2})], \end{aligned} \quad (30)$$

where

$$\tau_{1/2} = -\frac{1}{\gamma} \ln \left[\left(\frac{1}{2} - f \right) \left(\frac{(1 - m)P_0}{N_m} - f \right)^{-1} \right] > 0 \quad (31)$$

is the time required for the diagonal state to become passive ($P_m(\tau_{1/2}) = 1/2$), i.e., completely discharged. Finally, after some dissipation time τ , the reversal measurement is performed, restoring part of the ergotropy, such that $\mathcal{R}_{iv}^{\text{inc}} > \mathcal{R}_{iii}^{\text{inc}}$, where $\mathcal{R}_{iv}^{\text{inc}} = \mathcal{R}_{mw}^{\text{inc}}(\tau)$ is given

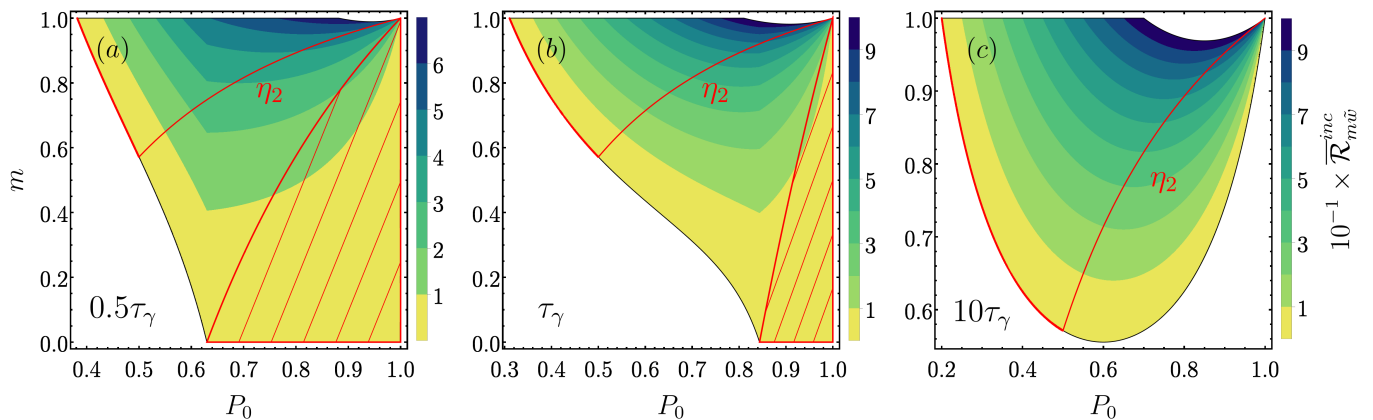


FIG. 2: **Incoherent ergotropy gain** as a function of the weak measurement strength m and initial population P_0 along the null energetic shift reversal measurement strength $\tilde{w} \in [0, 1]$ for distinct dissipation times (a) $\tau = 0.5\tau_\gamma$, (b) $\tau = \tau_\gamma$, and (c) $\tau = 10\tau_\gamma$. The red-hatched region and red curves indicate that $\mathcal{W}_{m\tilde{w}}(\tau) = 0$. The η_2 lines are highlighted.

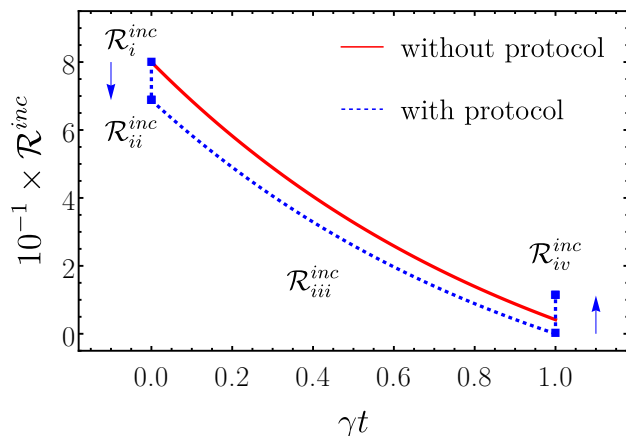


FIG. 3: **Incoherent ergotropy comparison.** Incoherent ergotropy changes with (dashed blue) and without (continuous red) the execution of the protocol for $P_0 = 0.9$, dissipation time $\tau = \tau_\gamma$, and strengths $m = 0.4$ and $w = \tilde{w} \approx 0.2$. The blue arrows highlight the incoherent ergotropy jumps due to the measurements.

by Eq. (13) for the incoherent component of the final ergotropy.

Along with null energy and ergotropy shifts, the protocol performance is characterized by the ergotropy gain, quantifying the amount of ergotropy saved, relative to a quantum battery subjected to a purely discharging process. In this context, Fig. 2 illustrates the behavior of incoherent ergotropy gain as a function of the weak measurement strength m and the initial population P_0 , computed along $\tilde{w} \in [0, 1]$ at various dissipation times: (a) $0.5\tau_\gamma$, (b) τ_γ , and (c) $10\tau_\gamma$. For clarity, the region where $\bar{\mathcal{R}}_{m\tilde{w}}^{inc}(\tau) \leq 0$ —indicating no gain following protocol execution—has been omitted. The red-hatched

areas and red curves denote operational regions where $\mathcal{W}_{m\tilde{w}}(\tau) = 0$. The red lines η_2 show points characterized by the equal-strength curve, as defined in Eq. (25). Notice that, in general, stronger measurements m yield higher gains. It is also evident that not all parameter space corresponds to valid operational regions. The size of these working regions depends strongly on the dissipation time τ , gradually decreasing over time and eventually saturating for long dissipation times, characterized by the reversal measurement strength $\lim_{\tau \rightarrow \infty} \tilde{w}$. In this regime, the only remaining valid execution of the protocol with a finite gain is characterized by η_2 .

To better illustrate how the protocol functions, Fig. 3 shows the variation of the incoherent ergotropy during each step (dashed-blue line), assuming $P_0 = 0.9$, $m = 0.4$, dissipation time $\tau = \tau_\gamma$, and $w = \tilde{w} \approx 0.2$, which ensure $\varepsilon_{m\tilde{w}}(\tau_\gamma) = 0$. This is compared to the purely discharging process (continuous-red line). The blue arrows indicate the discontinuous (instantaneous) ergotropy jumps caused by the weak and reversal measurements. According to Fig. 2b, the chosen parameters lie within the operational region, with $\mathcal{W}_{m\tilde{w}}(\tau_\gamma) = 0$. Note that while \hat{M}_m decreases the initial battery ergotropy, the execution of the final step, $\hat{W}_{\tilde{w}}$, increases it. Furthermore, the battery becomes nearly fully discharged due to environmental interaction at step (iii), since $\tau_\gamma \approx \tau_{1/2}$. As a result, at the end of the protocol, the final incoherent ergotropy \mathcal{R}_{iv}^{inc} exceeds the red curve, yielding $\bar{\mathcal{R}}_{m\tilde{w}}^{inc}(\tau_\gamma) \approx 0.71 \times 10^{-1}$. It is important to emphasize that this gain is achieved without actively introducing any additional external resources, which is ensured by an appropriate choice of parameters that results in null energetic and ergotropic shifts.

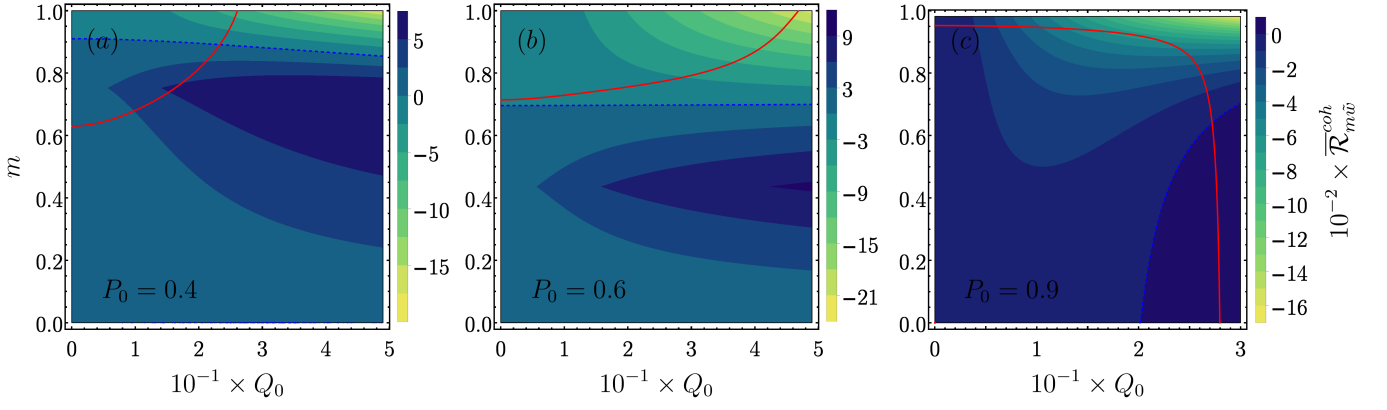


FIG. 4: **Coherent ergotropy gain** as a function of m and initial coherence $Q_0 \in [0, \sqrt{P_0(1-P_0)}]$ computed along $\bar{w} \in [0, 1]$ and τ_γ for (a) $P_0 = 0.4$, (b) $P_0 = 0.6$, (c) $P_0 = 0.9$. The dashed blue line represents the points where $\bar{\mathcal{R}}_{m\bar{w}}^{coh}(\tau_\gamma) = 0$. The red lines highlight the region where $\mathcal{W}_{m\bar{w}}(\tau) = 0$.

B. Coherent ergotropy

The role played by the coherence for the protocol is fully encoded into Eq. (15). Since the measurement operations are incoherent, this quantity is non-null iff $Q_0 \neq 0$. Hence, given $\hat{\rho}_0$, the initial coherent component of the ergotropy is written as

$$\mathcal{R}_i^{coh} = \frac{1}{2} \left(-|1 - 2P_0| + \sqrt{(1 - 2P_0)^2 + 4|Q_0|^2} \right). \quad (32)$$

After performing the weak measurement at step (ii), the ergotropy jumps to

$$\begin{aligned} \mathcal{R}_{ii}^{coh} = & -\frac{|2 - 2P_0 - N_m|}{2N_m} \\ & + \frac{\sqrt{(2 - 2P_0 - N_m)^2 - 4|Q_0|^2 \frac{(1 - P_0 - N_m)}{P_0}}}{2N_m}. \end{aligned} \quad (33)$$

In contrast to the incoherent counterpart, the behavior of coherent ergotropy during the interaction with the environment is more complex. See Appendix A for more details. Specifically, the coherent ergotropy does not necessarily decay monotonically over time, even though $Q_m(t)$ exhibits monotonic behavior. Therefore, during step (iii), one has

$$\begin{aligned} \mathcal{R}_{iii}^{coh} = & -\frac{1}{2}|1 - 2P_m(t)| \\ & + \frac{1}{2}\sqrt{(1 - 2P_m(t))^2 + 4|Q_m(t)|^2}. \end{aligned} \quad (34)$$

Finally, after the reversal measurement at step (iv), the coherent ergotropy becomes

$$\begin{aligned} \mathcal{R}_{iv}^{coh} = & -\frac{|N_{mw}(\tau) - 2P_m(\tau)|}{2N_{mw}(\tau)} \\ & + \frac{\sqrt{(N_{mw}(\tau) - 2P_m(\tau))^2 + \frac{4|Q_m(\tau)|^2(P_m(\tau) - N_{mw}(\tau))}{(P_m(\tau) - 1)}}}{2N_{mw}(\tau)}. \end{aligned} \quad (35)$$

To provide a broader characterization of the role of coherence, Fig. 4 illustrates the landscape of coherent ergotropy gain in terms of m and initial coherence $Q_0 \in [0, \sqrt{P_0(1-P_0)}]$. This is computed along $\bar{w} \in [0, 1]$ at τ_γ for fixed initial populations: (a) $P_0 = 0.4$, (b) $P_0 = 0.6$, and (c) $P_0 = 0.9$. As before, the red lines indicate the working points, where $\mathcal{W}_{m\bar{w}}(\tau) = 0$. It is evident that, depending on the parameters, coherence can offer an advantage to the protocol and contribute positively to the ergotropy gain. Nevertheless, at $P_0 = 0.6$, no combination of Q_0 and m yields a $\bar{\mathcal{R}}_{m\bar{w}}^{coh}(\tau_\gamma) > 0$ at operational points. Still, it is noteworthy that its scale is one order of magnitude lower than the incoherent part, suggesting that the overall protocol may still be beneficial despite small negative contributions. Also, notice that, given the monotonic decay of the coherence independently of the protocol, no gain is anticipated for long dissipation times. In this sense, Fig. 5 complements Fig. 4b and Fig. 4c by showing how the coherent ergotropy gain behaves in terms of τ for different measurement strengths m and $\bar{w} \in [0, 1]$, assuming maximum real value allowed for each P_0 , given by $Q_0 = Q_{max} := \sqrt{P_0(1-P_0)}$ for (a) $P_0 = 0.6$, (b) $P_0 = 0.9$. It is possible to see that, for small τ , the operational values of m change. After that, it asymptotically approaches a stationary value.

Finally, as an illustrative example, Fig. 6 displays how the coherent ergotropy changes at each step of the protocol, assuming the same set of parameters used in Fig. 3 with the additional initial coherence $Q_0 \approx 0.28$ to achieve an operational point (see Fig. 4c). As previously mentioned, this quantity exhibits non-trivial behavior during the environmental interaction. Namely, one can show that for $P_0 > 1/2$, \mathcal{R}_{iii}^{coh} increases over time, reaching a turning point at $\tau_{1/2}$ given by Eq. (31), when the diagonal state becomes passive. Given that $\tau_\gamma \approx \tau_{1/2}$ for the chosen parameters, such non-monotonicity is not observed. Also, in contrast to the incoherent part, the action of \hat{M}_m and $\hat{W}_{\bar{w}}$ respectively increase and decrease the coherent

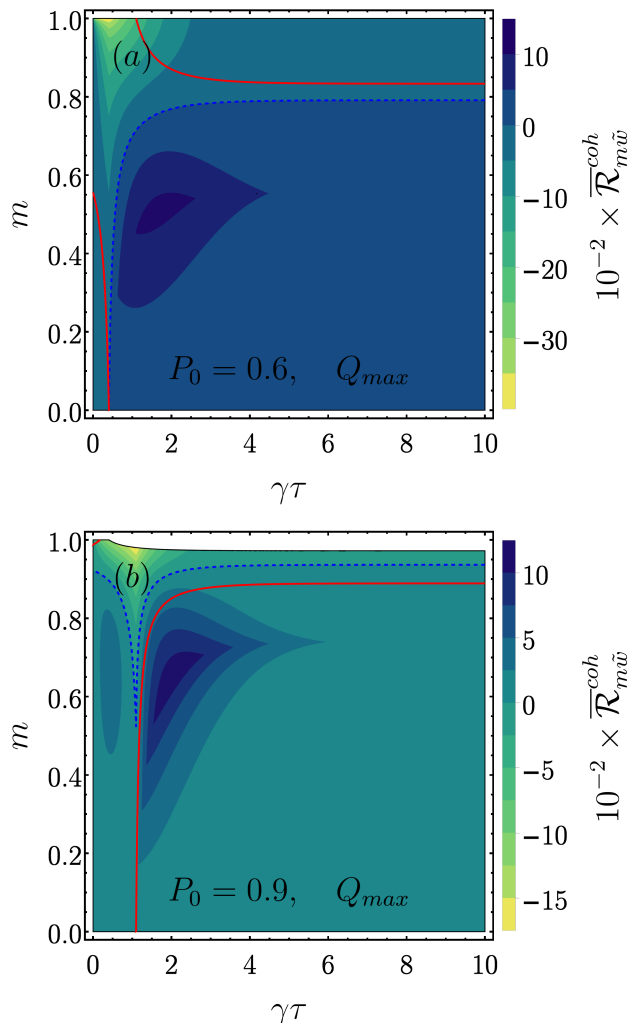


FIG. 5: **Coherent ergotropy gain** in terms of dissipation time and measurement strength m for (a) $P_0 = 0.6$ and (b) $P_0 = 0.9$, assuming $Q_0 = Q_{\text{max}}$ and $\tilde{w} \in [0, 1]$. The blue dashed lines represent the points with null coherent ergotropy gain. The red curves indicate the operational points, where $\mathcal{W}_{m\tilde{w}}(\tau) = 0$.

ergotropy. Despite that, at the end of the protocol $\mathcal{R}_{i\tilde{w}}^{\text{coh}}$ still remains above the red curve, resulting in a small finite gain of $\overline{\mathcal{R}}_{m\tilde{w}}^{\text{coh}}(\tau_\gamma) \approx 0.5 \times 10^{-2}$.

It is important to highlight that, although the incoherent and coherent components of the ergotropy gain behave differently according to the protocol parameters, the post-selection probabilities—and therefore the success probability—for a coherent battery and an equivalent incoherent one (with the same diagonal states) remain the same. In the following analysis, we examine the total ergotropy gain alongside the success probability to assess how likely it is to achieve the desired post-selections, while also weighing this against the benefits of mitigating the discharging dynamics.

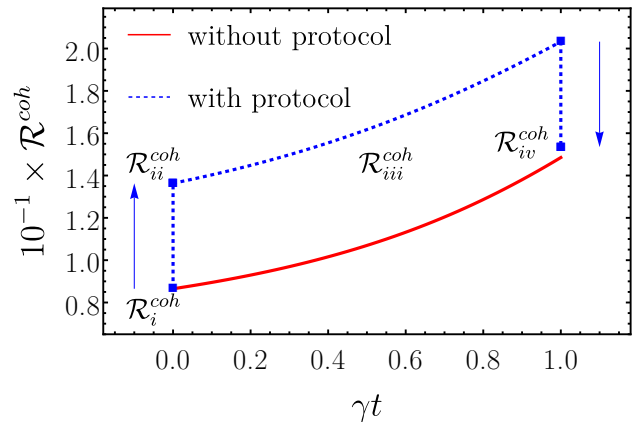


FIG. 6: **Coherent ergotropy comparison.** Coherent ergotropy changes with (dashed blue) and without (continuous red) the execution of the protocol for the same parameters used in Fig. 3 and $Q_0 \approx 0.28$. The blue arrows highlight the coherent ergotropy jumps due to the measurements.

C. Total ergotropy gain and success probability

To better assess the general performance of the protocol, Fig. 7 presents (a) the total and (b) coherent ergotropy gains landscape in terms of the initial population P_0 and the weak measurement strength m , and (c) the probability of success. These quantities were computed along $\tilde{w} \in [0, 1]$, dissipation time $\tau = \tau_\gamma$ and for the initial coherence it was assumed $Q_0 = Q_{\text{max}}$ for each P_0 . The blue dashed lines represent the points where the ergotropy gains are null, while the red continuous line highlights the protocol's working points, where $\mathcal{W}_{m\tilde{w}}(\tau_\gamma) = 0$ is also satisfied. Notice that, despite the total ergotropy gain being positive for most of the $P_0 \times m$ surface, for the chosen set of parameters the protocol has no operational points above a certain value of $P_0 \approx 0.85$. Also, it is possible to observe that one obtains higher gains for stronger measurements, even in regions where the coherence contribution is negative. As a probabilistic protocol, its performance should be evaluated alongside its probability of success. In this sense, notice that $\overline{\mathcal{R}}_{m\tilde{w}}(\tau_\gamma)$ and $\Pi_{m\tilde{w}}(\tau_\gamma)$ are inversely related, i.e., higher gains are obtained with lower probabilities of success and vice versa. On the other hand, the coherent ergotropy gain has a positive contribution with higher probabilities. It should be stressed that the observed probability landscape is a generic feature of the protocol, due to its independence of the initial coherence Q_0 , i.e., the fact that the probability is maximized in the direction of lower m and P_0 is observed regardless of the amount of coherence initially assumed. To better understand the relationship between gain and probability, Fig. 8 illustrates the probability of success as a function of the ergotropy gain and P_0 for measurement strengths $m = 0.1$, $m = 0.5$, and $m = 0.9$,

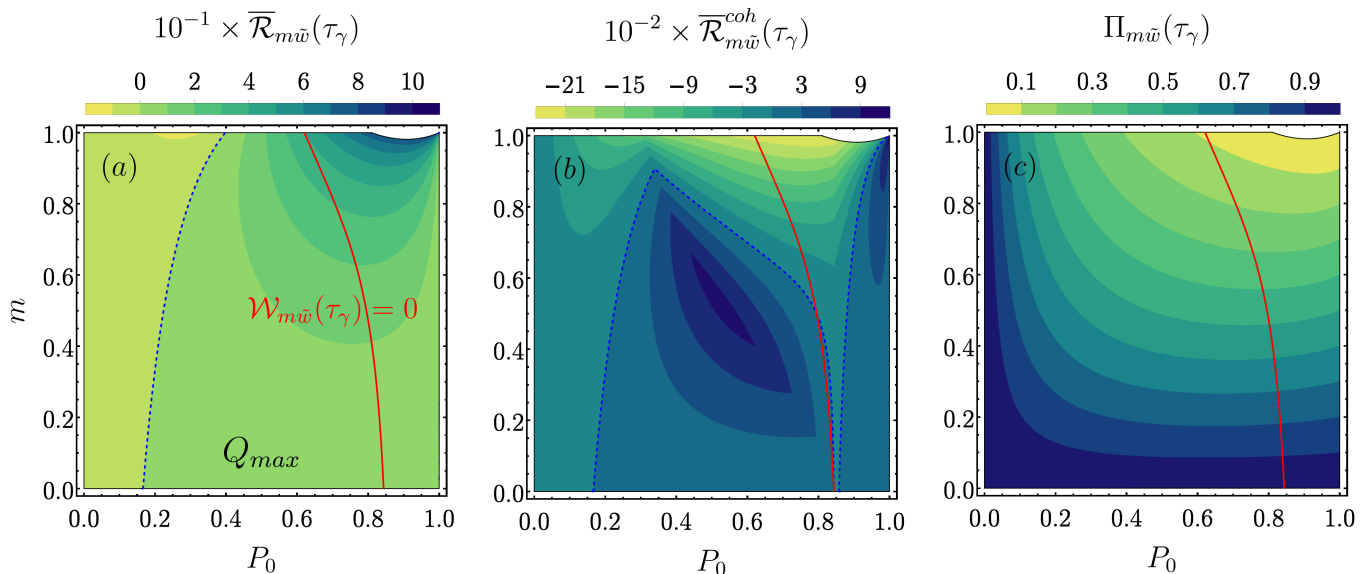


FIG. 7: **Protocol performance** in terms of the weak measurement strength m and initial population P_0 . These quantities were computed along the null energetic shift curve $\tilde{w} \in [0, 1]$, considering $Q_0 = Q_{max}$ for each P_0 , and $\tau = \tau_\gamma$. The dashed blue curves indicate the points with null ergotropy gain, while the red lines highlight the points satisfying $\mathcal{W}_{m\tilde{w}}(\tau_\gamma) = 0$. (a) Total ergotropy gain; (b) Coherence contribution to the protocol, quantified by the coherent ergotropy gain; (c) Protocol's success probability.

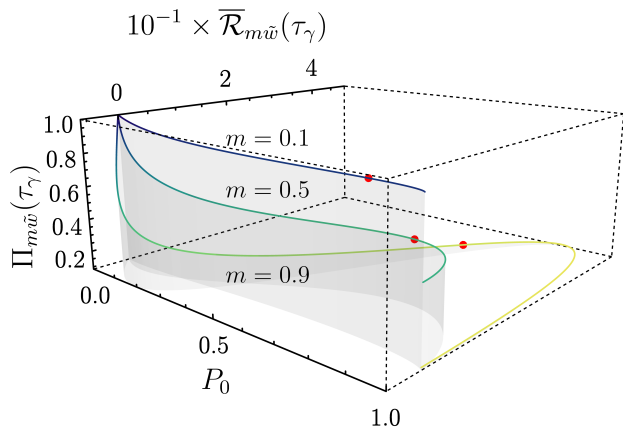


FIG. 8: **Success probability** in terms of the ergotropy gain and P_0 for $m = 0.1$, $m = 0.5$ and $m = 0.9$, computed at τ_γ , $\tilde{w} \in [0, 1]$ and $Q_0 = Q_{max}$ for each P_0 . The red dots represent the operational points of each curve, where $\mathcal{W}_{m\tilde{w}}(\tau_\gamma) = 0$.

assuming $Q_0 = Q_{max}$ for each P_0 . The red dots denote the working points of each curve, where $\mathcal{W}_{m\tilde{w}}(\tau_\gamma) = 0$ is also satisfied. Notably, for $m = 0.1$, a small gain is achieved with a high probability, whereas for $m = 0.9$, the gain is significantly higher but comes at the cost of a much lower probability, indicating an inverse relationship between these two quantities. Therefore, by tuning to intermediate measurement strengths, it is possible to identify operational points that balance finite gain with

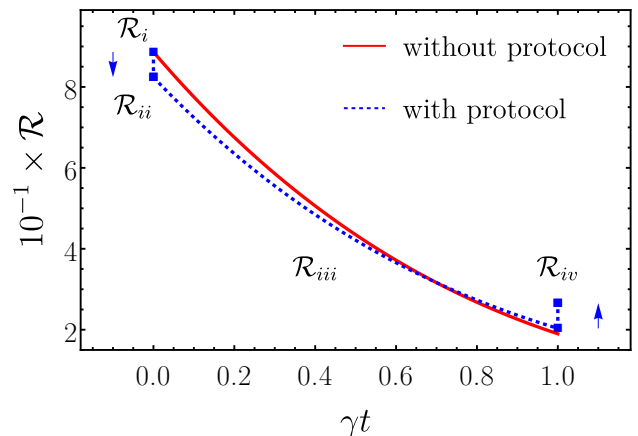


FIG. 9: **Ergotropy comparison.** Ergotropy changes with (dashed blue) and without (continuous red) the execution of the protocol for $P_0 = 0.9$, $Q_0 \approx 0.28$, dissipation time $\tau = \tau_\gamma$, and strengths $m = 0.4$ and $w = \tilde{w} \approx 0.20$. The blue arrows highlight the ergotropy jumps due to the measurements. The probability of success is $\Pi_{m\tilde{w}}(\tau_\gamma) \approx 0.57$.

effective probability.

The total ergotropy changes induced during the protocol, composed of both the incoherent and coherent components, are depicted in Fig. 9 for the same parameters introduced previously. Note that, in this case, the resulting battery discharging process after the weak measurement (dashed blue line) is slower than the one ob-

tained without performing it (continuous red line). Such a difference in ergotropy loss leads to the crossing of both curves and, ultimately, more ergotropy is saved after some dissipation time. Nevertheless, despite satisfying the constrain $\varepsilon_{m\bar{w}}(\tau_\gamma) = \mathcal{W}_{m\bar{w}}(\tau_\gamma) = 0$, the reversal measurement gives even more ergotropy to the battery, providing a positive gain at the end of the protocol of $\bar{\mathcal{R}}_{mw}(\tau_\gamma) \approx 0.76 \times 10^{-1}$. The probability of success for this particular example is $\Pi_{m\bar{w}}(\tau_\gamma) \approx 0.57$.

IV. DISCUSSION

Given recent advancements in quantum thermodynamics [100] and the growing ability to manipulate quantum systems [77], the development of quantum technologies for energy control and management has become increasingly crucial [101–104]. In this context, the design and analysis of efficient quantum devices for energy storage have gained significant interest, with proposals across different physical platforms [5, 23, 25–32]. Nevertheless, due to the fragile nature of quantum systems, realistic implementations must consider environmental interactions, which often lead to unwanted discharging. Developing methods to counteract such discharge effect has thus become a key focus for practical quantum battery applications, and this work contributes to this ongoing effort.

Here, we introduced a protocol for mitigating the inevitable discharging process in a single qubit open quantum battery by applying two selective weak measurements. More specifically, a first weak measurement is performed right after the battery charging -before being subjected to environmental interaction-, followed by a reversal measurement after some dissipation time. The protocol’s operating points were set by thermodynamic constrains, namely by simultaneously meeting the conditions $\varepsilon_{mw}(\tau) = 0$ and $\mathcal{W}_{mw}(\tau) = 0$, which respectively define the proper parameter space for minimum external energetic and ergotropic influences. Such conditions can be achieved due to the symmetry of the weak measurement and its reversal. In this way, we showed that by properly executing the protocol, one can obtain positive gain, i.e., the final ergotropy can be higher compared to a purely discharged quantum battery, effectively mitigating the effects of environmental interactions. Nevertheless, it is worth mentioning the previous constraints can be relaxed, provided the ergotropy shift $\mathcal{W}_{mw}(\tau)$ remains below the protocol-induced ergotropy gain; in other words, even allowing for small extra recharging from the measurements can be advantageous, depending on the success probability. In the more restrictive case—where both measurements result in zero energy and ergotropy shifts—we analyzed the differences in behavior for the incoherent and coherent components of ergotropy.

Our results demonstrate that quantum coherence can be analyzed separately to optimize the performance of the protocol, allowing for better conditions for both the ergotropy gain and the probability of success. The opti-

mal setup will naturally depend on the specific characteristics of the battery system and the environment. Our work characterizes a general scenario to facilitate adaptation to specific applications.

To demonstrate our method, we selected specific parameter examples. Since any quantum system decays over the time scale determined by the dissipation rate into the environment, we concentrated on the energy (ergotropy) mitigation in the period of $\tau_\gamma = 1/\gamma$. We observed that achieving higher ergotropy gains comes at the cost of lower probabilities of success, and vice versa, indicating an inverse relationship. Notably, the success probability landscape of the protocol remains invariant with respect to the initial coherence. Through our examples, we demonstrated how the coherent ergotropy gain can positively contribute at higher probabilities, showcasing how quantum features like coherence can be effectively harnessed to enhance the protocol’s overall performance.

The results presented here can be straightforwardly expanded to consider a protocol for multi-qubit batteries, exploring whether the obtained gain scale with an increasing number of systems (cells). This would involve considering the role played by the internal coupling between different cells of the battery and determining how interactions among qubits might affect overall performance. Additionally, it would be valuable to understand how quantum correlations such as entanglement and quantum discord [105, 106] behave within this weak measurement-based protocol, especially as it could impact both the stability and efficiency of the quantum battery. Examining the energetic cost of measurements, following Landauer’s principle, would also be important, as this would provide insights into the thermodynamic cost associated with implementing the weak measurements, allowing for a more comprehensive assessment of the protocol’s practicality.

Finally, optimal parameter choices for successfully applying the protocol will likely depend on system-specific and environmental constraints. In realistic setups, it may not always be possible to control factors like dissipation time, temperature or to precisely modulate measurement strength, which could limit the achievable gains. Future work should consider these constraints and investigate adaptive protocols that can respond to variable conditions, enabling the practical application of this approach across a wider range of quantum battery designs and operational environments.

V. ACKNOWLEDGEMENTS

The authors thank Michał Horodecki and Paweł Mazurek for the valuable discussions and suggestions. A.H.A.M. and R.S. acknowledge support from National Science Centre, Poland Grant OPUS-21 (No. 2021/41/B/ST2/03207). B.A. acknowledges support from National Science Center, Poland within the QuantERA II Programme (No 2021/03/Y/ST2/00178,

acronym ExTRaQT) that has received funding from the European Union's Horizon 2020. P.R.D. acknowledges support from the NCN Poland, ChistEra-2023/05/Y/ST2/00005 under the project Modern Device Independent Cryptography (MoDIC).

Appendix A: Dissipation and battery discharging

In the basis $\{|g\rangle, |e\rangle\}$, the density matrix of the battery is written as

$$\hat{\rho}(t) = \begin{pmatrix} 1 - P(t) & Q(t) \\ Q^*(t) & P(t) \end{pmatrix}. \quad (\text{A1})$$

Eq. (3) provides its time-evolution when the battery is exposed to an environment with the inverse of temperature β . In this case, it is straightforward to obtain the following set of uncoupled differential equations for the matrix elements $P(t)$ and $Q(t)$:

$$\begin{aligned} \frac{d}{dt}P(t) &= \gamma(f - P(t)), \\ \frac{d}{dt}Q(t) &= -\frac{1}{2}Q(t)(\gamma - 2i\omega), \end{aligned} \quad (\text{A2})$$

such that

$$\begin{aligned} P(t) &= (P_0 - f)e^{-\gamma t} + f, \\ Q(t) &= Q_0 e^{-\frac{\gamma t}{2} + it\omega}, \end{aligned} \quad (\text{A3})$$

where P_0 and Q_0 represent the initial population of the excited state and the initial coherence, respectively. It is important to note that these quantities evolve independently over time, without any coupling between them. Furthermore, in the long time limit ($t \rightarrow \infty$) we have $P_\infty = f$ and $Q_\infty = 0$, i.e.,

$$\lim_{t \rightarrow \infty} \hat{\rho}(t) = \hat{\tau}_{\text{th}}, \quad (\text{A4})$$

where $\hat{\tau}_{\text{th}} := (1 - f)|g\rangle\langle g| + f|e\rangle\langle e|$ is the thermal (Gibbs) state relative to β . Thus, it is clear that energy is irreversibly leaked into the environment during the battery thermalization, leading to its inevitable discharge.

This phenomenon is illustrated in Fig. 10 for various coherent and incoherent initial states, characterized by P_0 and Q_0 . Notably, when the initial state is active, the ergotropy decreases monotonically and irreversibly over time. In contrast, for passive states, the ergotropy remains constant and zero, as indicated by the red dashed line. Additionally, note that the discharging rates vary significantly. For instance, in the case of a fully charged battery, represented by the solid black line, the decay is faster than for initially coherent states. From this perspective, certain partially charged initial states may retain more ergotropy after a period of dissipation, presenting a potential advantage. This counterintuitive behavior arises from the complex interplay between the incoherent and coherent components of ergotropy during thermalization.

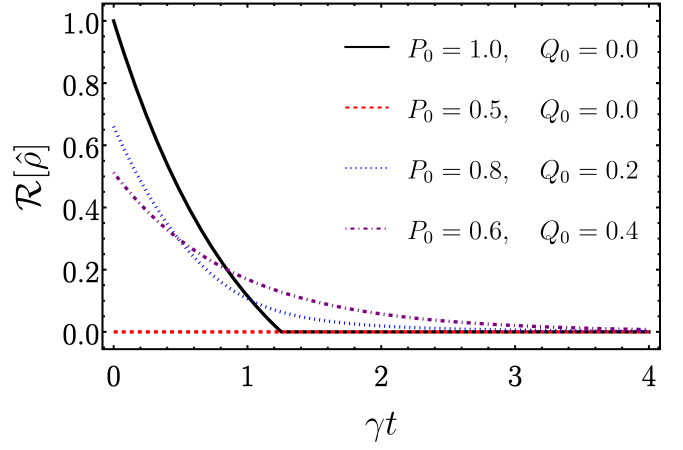


FIG. 10: **Discharging process:** Ergotropy behavior as a function of the dissipation time for distinct initial states, characterized by P_0 and Q_0 . It was assumed $\omega = 1$, $f = 0.3$ and $\gamma = 10^{-2}$.

In such a scenario, the evolution of the incoherent ergotropy reads

$$\begin{aligned} \mathcal{R}^{\text{inc}}[\hat{\rho}(t)] &= \omega (2P(t) - 1) [1 - \Theta(1/2 - P_0)] \\ &\quad \times [1 - \Theta(t - \tau_{1/2})], \end{aligned} \quad (\text{A5})$$

where $\Theta(x)$ is the Heaviside function, such that $\Theta(x) = 1$ if $x \geq 0$ and null otherwise, and

$$\tau_{1/2} := -\frac{1}{\gamma} \ln \left[\left(\frac{1}{2} - f \right) (P_0 - f)^{-1} \right] \quad (\text{A6})$$

is the time instant when the diagonal state of the battery becomes passive ($P(\tau_{1/2}) = 1/2$) and the ergotropy reaches zero. In this sense, Fig. 11 shows the incoherent ergotropy landscape behavior relative to the dissipation time and initial population. For initially active diagonal states ($P_0 > 1/2$), the monotonicity of the ergotropy is evident. The dashed red line highlights the points where the battery is fully discharged, defined by $\tau_{1/2}$.

On the other hand the coherent ergotropy at time t is written as [97, 98]

$$\mathcal{R}^{\text{coh}}[\hat{\rho}(t)] = \frac{1}{2} \left(\psi(t) - \sqrt{\psi^2(t) - 4|Q(t)|^2} \right), \quad (\text{A7})$$

where $\psi(t) = \sqrt{2\mu[\hat{\rho}(t)] - 1}$, with $\mu[\hat{\rho}] := \text{Tr}[\hat{\rho}^2]$ being the purity of the state $\hat{\rho}$. The Eq. (A7) above possesses a less trivial structure and dynamics, despite clearly approaching zero for $t \rightarrow \infty$, i.e., one can show that

$$\psi^2(t) - 4|Q(t)|^2 = 4(P_0 - f)^2 \frac{\left(1 - e^{\gamma(t - \tau_{1/2})}\right)^2}{e^{2\gamma t}}, \quad (\text{A8})$$

which is monotonic in time t for $P_0 \leq 1/2$ and non-monotonic otherwise. In the latter case, the minimum value is reached at the time $\tau_{1/2}$, satisfying $\psi^2(\tau_{1/2}) -$

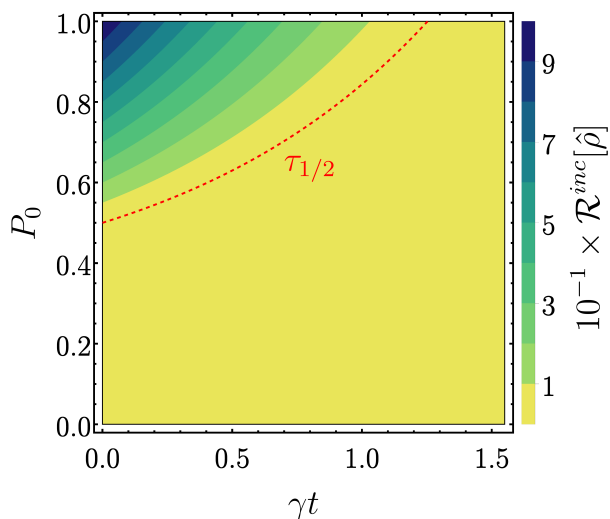


FIG. 11: **Incoherent ergotropy** in terms of the dissipation time and initial population P_0 . The dashed red line highlights the curve $\tau_{1/2}$, representing the instant where the diagonal state becomes passive ($P(\tau_{1/2}) = 1/2$). It was assumed $\omega = 1$, $f = 0.3$, $\gamma = 10^{-2}$.

$4|Q(\tau_{1/2})|^2 = 0$. This time dependency leads to a non-monotonic evolution of the coherent ergotropy $\mathcal{R}^{coh}[\hat{\rho}(t)]$, meaning that, despite interaction with the environment, the coherent ergotropy may initially increase before its inevitable decrease. This behavior has a direct impact on the battery's discharging rate. Figure 12 illustrates the landscape of coherent ergotropy as a function of dissipation time and initial coherence $Q_0 \in [0, \sqrt{P_0(1-P_0)}]$ for (a) $P_0 = 0.2$ and (b) $P_0 = 0.8$. The dashed red lines indicate the curves $\tau_{1/2}$. As expected, in Fig. 12a, the coherent ergotropy decays monotonically over time. In contrast, in Fig. 12b, the previously described behavior is observed: $\mathcal{R}^{coh}[\hat{\rho}(t)]$ increases over $t \in [0, \tau_{1/2}]$, followed by a subsequent decay for $t > \tau_{1/2}$. It is also noteworthy that the contribution of the coherent component to the total ergotropy is smaller than that of the incoherent component.

In short, although the discharging process due to environmental interaction has a relatively straightforward description, the decay of total ergotropy arises from a complex interplay between the incoherent and coherent components. While the incoherent component exhibits monotonic behavior, the coherent component may show a non-trivial time dependency within certain parameter ranges.

Appendix B: Energy and ergotropy shifts

By design, the described protocol requires applying \hat{M}_m and \hat{W}_w to the battery state before and after some dissipation time. Both actions inherently cause energetic changes, resulting in additional charging or discharging

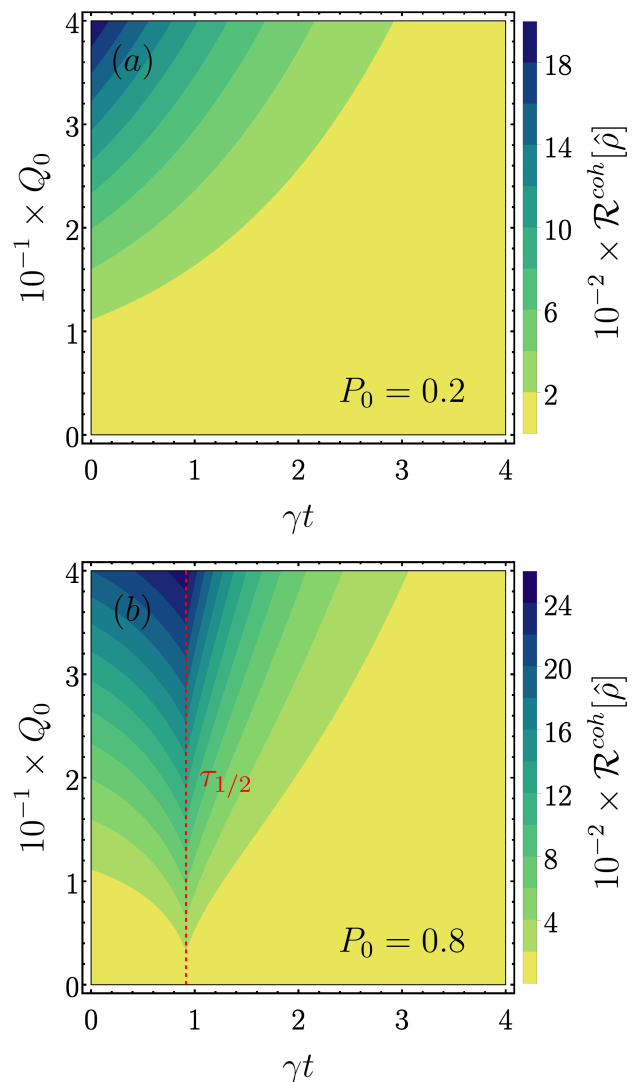


FIG. 12: **Coherent ergotropy** in terms of the dissipation time and initial coherence $Q_0 \in [0, \sqrt{P_0(1-P_0)}]$ for (a) $P_0 = 0.2$ and (b) $P_0 = 0.8$. The dashed red line highlights the curve $\tau_{1/2}$. It was assumed $\omega = 1$, $f = 0.3$, $\gamma = 10^{-2}$.

of the battery. To ensure minimal external disturbance, it is essential that no net energy or ergotropy is imparted. In other words, the valid working regime of the protocol should be constrained to parameters that simultaneously satisfy $\varepsilon_{mw}(\tau) = 0$ and $\mathcal{W}_{mw}(\tau) = 0$. For fixed values of γ , f , P_0 , m , and τ , the former condition can be achieved by adjusting the reversal measurement strength to \tilde{w} , as defined in Eq. (24). Figure 13 illustrates the behavior of the \tilde{w} -surface for null energetic shift in terms of the initial excited population P_0 and strength m , evaluated at $\tau = \tau_\gamma$. The suppressed region represents non-physical values of measurement strength, where $\tilde{w} \notin [0, 1]$. Higher values of \tilde{w} are required as m increases and for intermediate values of P_0 . Since the post-weak measurement state remains invariant under the action of \hat{M}_m for $P_0 = 0, 1$

(implying $Q_0 = 0$), no energy is transferred during the initial measurement, so $\tilde{w} = 0$ is sufficient to ensure $\varepsilon_{m\tilde{w}}(\tau) = 0$. These general characteristics hold for different dissipation times τ . Notably, for long times, the \tilde{w} -surface converges

$$\lim_{\tau \rightarrow \infty} \tilde{w} = \frac{(1 - P_0)(1 - N_m)}{(1 - f)[(1 - P_0)(1 - N_m) + fN_m]}. \quad (\text{B1})$$

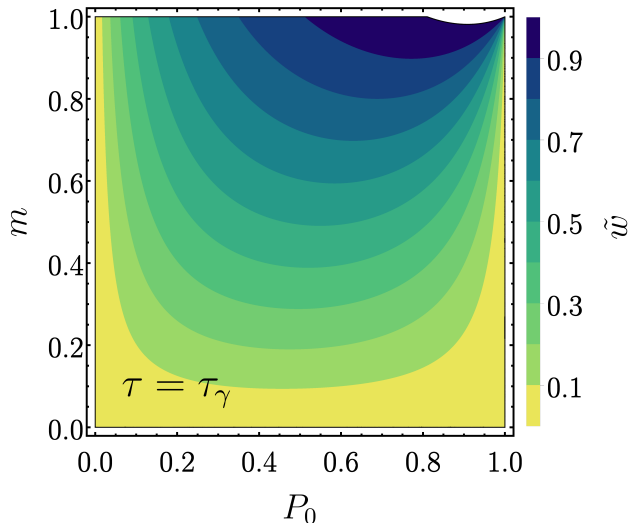


FIG. 13: **Null energetic shift surface** in terms of P_0 and m , computed at τ_γ . The non-physical region, $\tilde{w} \notin [0, 1]$, is suppressed. It was assumed $f = 0.3$ and $\gamma = 10^{-2}$.

Nevertheless, given that $\varepsilon_{m\tilde{w}}(\tau) = 0$, it remains necessary to identify parameters that also satisfy $\mathcal{W}_{m\tilde{w}}(\tau) = 0$. To illustrate this, Fig. 14 presents the energetic shift profile across different parameter settings. Figures 14a–c display the behavior of the profile with respect to the

reversal measurement strength w and the dissipation time τ , assuming an initial coherence $Q_0 = Q_{max} := \sqrt{P_0(1 - P_0)}$ and weak measurement strength $m = 0.5$, for different initial population values: (a) $P_0 = 0.4$, (b) $P_0 = 0.8$, and (c) $P_0 = 0.9$. As expected, most of the parameter space shows a non-zero net energetic exchange. However, the intersection of the dashed black and continuous red curves marks the operational points of the protocol. The former indicates a null energetic shift, characterized by \tilde{w} , while the latter identifies points where $\mathcal{W}_{mw}(\tau) = 0$ holds. For the chosen parameters, these intersections may only occur at specific dissipation times.

Similarly, Figs. 14d–f present the energy shift landscape for the same initial populations, assuming $Q_0 = 0$ and equal measurement strengths, $m = w = \eta$. The dashed black lines mark points defined by the null energetic shift curves $\eta_{2,3}$, while the continuous red lines and hatched red areas highlight where a null ergotropy shift is obtained. Again, the intersections represent the desired working regime. As discussed in the main text, the η_2 curve for incoherent states leads to a cyclic transformation, $\hat{\rho}_0 \rightarrow \hat{\tau}_{th} \rightarrow \hat{\rho}_0$, ensuring that the battery state remains unchanged during dissipation, thus satisfying $\varepsilon_{\eta_2\eta_2} = \mathcal{W}_{\eta_2\eta_2} = 0$ for all τ . However, for the selected parameters, the η_3 curve does not exhibit any operational points.

It is important to emphasize that Fig. 14 serves as a proof-of-concept illustration of the proposed protocol. The operational points depend heavily on the selected values. Nevertheless, some general insights can be observed: (i) a finite energetic change exists over most of the parameter space; (ii) the conditions required to minimize external influence significantly constrain the working regime. Nonetheless, it is still possible to identify intersection points where $\varepsilon_{mw}(\tau) = 0$ and $\mathcal{W}_{mw}(\tau) = 0$ are simultaneously satisfied. Therefore, in principle, even with additional external constraints in experimental scenarios (such as temperature or measurement strength), it is feasible to adapt the protocol accordingly.

-
- [1] R. Alicki and M. Fannes, Entanglement boost for extractable work from ensembles of quantum batteries, *Phys. Rev. E* **87**, 042123 (2013).
 - [2] F. C. Binder, S. Vinjanampathy, K. Modi, and J. Goold, Quantacell: powerful charging of quantum batteries, *New Journal of Physics* **17**, 075015 (2015).
 - [3] T. P. Le, J. Levinsen, K. Modi, M. M. Parish, and F. A. Pollock, Spin-chain model of a many-body quantum battery, *Phys. Rev. A* **97**, 022106 (2018).
 - [4] F. Campaioli, S. Gherardini, J. Q. Quach, M. Polini, and G. M. Andolina, Colloquium: Quantum batteries, *Rev. Mod. Phys.* **96**, 031001 (2024).
 - [5] J. Q. Quach, K. E. McGhee, L. Ganzer, D. M. Rouse, B. W. Lovett, E. M. Gauger, J. Keeling, G. Cerullo, D. G. Lidzey, and T. Virgili, Superabsorption in an organic microcavity: Toward a quantum battery, *Science advances* **8**, 3160 (2022).
 - [6] G. M. Andolina, D. Farina, A. Mari, V. Pellegrini, V. Giovannetti, and M. Polini, Charger-mediated energy transfer in exactly solvable models for quantum batteries, *Phys. Rev. B* **98**, 205423 (2018).
 - [7] J. Monsel, M. Fellous-Asiani, B. Huard, and A. Auffèves, The energetic cost of work extraction, *Phys. Rev. Lett.* **124**, 130601 (2020).
 - [8] B. i. e. i. f. m. c. Çakmak, Ergotropy from coherences in an open quantum system, *Phys. Rev. E* **102**, 042111 (2020).
 - [9] S. Seah, M. Perarnau-Llobet, G. Haack, N. Brunner, and S. Nimmrichter, Quantum speed-up in collisional battery charging, *Phys. Rev. Lett.* **127**, 100601 (2021).
 - [10] R. Salvia, M. Perarnau-Llobet, G. Haack, N. Brunner, and S. Nimmrichter, Quantum advantage in charging cavity and spin batteries by repeated interactions, *Phys. Rev. Res.* **5**, 013155 (2023).

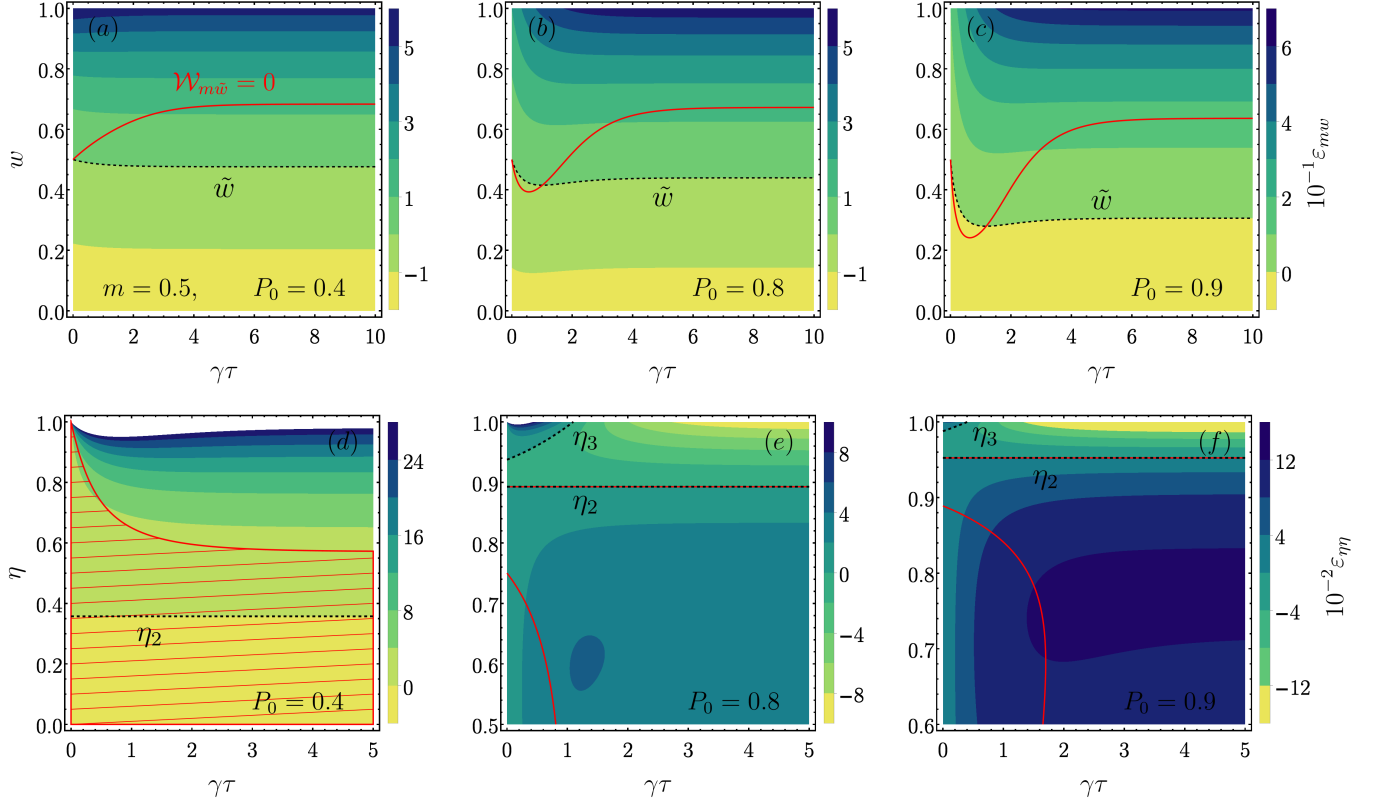


FIG. 14: **Energy shift profile.** (a)-(c) Energy shift in terms of the reversal strength w and dissipation time τ , assuming fixed strength $m = 0.5$ and $Q_0 = Q_{max} := \sqrt{P_0(1 - P_0)}$, for (a) $P_0 = 0.4$, (b) $P_0 = 0.8$ and (c) $P_0 = 0.9$. The dashed black lines represent the points along \tilde{w} , given by Eq. (24), where $\varepsilon_{mw}(\tau) = 0$, while the continuous red curves highlight where $\mathcal{W}_{mw}(\tau) = 0$. (d)-(f) Energy shift for equal measurement strengths $m = w = \eta$ relative to τ , assuming $Q_0 = 0$ for (d) $P_0 = 0.4$, (e) $P_0 = 0.8$ and (f) $P_0 = 0.9$. The black dashed lines represent the curves η_2 and η_3 for a null energetic shift, given by Eq. (25). The hatched red region and continuous red curves represent the points where $\mathcal{W}_{mw}(\tau) = 0$ is satisfied. It was assumed $\omega = 1$, $f = 0.3$, $\gamma = 10^{-2}$.

- [11] A. Glicenstein, G. Ferioli, A. Browaeys, and I. Ferrier-Barbut, From superradiance to subradiance: exploring the many-body dicke ladder, *Opt. Lett.* **47**, 1541 (2022).
- [12] B. Ahmadi, P. Mazurek, P. Horodecki, and S. Barzanjeh, Nonreciprocal quantum batteries, *Phys. Rev. Lett.* **132**, 210402 (2024).
- [13] B. Ahmadi, P. Mazurek, S. Barzanjeh, and P. Horodecki, Super-optimal charging of quantum batteries via reservoir engineering, *arXiv:2407.16553* (2024).
- [14] F. Barra, K. V. Hovhannisyanyan, and A. Imparato, Quantum batteries at the verge of a phase transition, *New Journal of Physics* **24**, 015003 (2022).
- [15] V. Shaghghi, V. Singh, G. Benenti, and D. Rosa, Micromasers as quantum batteries, *Quantum Science and Technology* **7**, 04LT01 (2022).
- [16] V. Shaghghi, V. Singh, M. Carrega, D. Rosa, and G. Benenti, Lossy micromaser battery: Almost pure states in the jaynes-cummings regime, *Entropy* **25**, 430 (2023).
- [17] Z.-G. Lu, G. Tian, X.-Y. Lü, and C. Shang, Topological quantum batteries, *arXiv:2405.03675* (2024).
- [18] E. Dennis, A. Kitaev, A. Landahl, and J. Preskill, Topological quantum memory, *Journal of Mathematical Physics* **43**, 4452 (2002).
- [19] R. R. Rodríguez, B. Ahmadi, P. Mazurek, S. Barzanjeh, R. Alicki, and P. Horodecki, Catalysis in charging quantum batteries, *Phys. Rev. A* **107**, 042419 (2023).
- [20] F. Kamin, F. Tabesh, S. Salimi, F. Kheirandish, and A. C. Santos, Non-markovian effects on charging and self-discharging process of quantum batteries, *New Journal of Physics* **22**, 083007 (2020).
- [21] R. R. Rodríguez, B. Ahmadi, G. Suárez, P. Mazurek, S. Barzanjeh, and P. Horodecki, Optimal quantum control of charging quantum batteries, *New Journal of Physics* **26**, 043004 (2024).
- [22] F. Mazzoncini, V. Cavina, G. M. Andolina, P. A. Erdman, and V. Giovannetti, Optimal control methods for quantum batteries, *Phys. Rev. A* **107**, 032218 (2023).
- [23] C.-K. Hu, J. Qiu, P. J. P. Souza, J. Yuan, Y. Zhou, L. Zhang, J. Chu, X. Pan, L. Hu, J. Li, Y. Xu, Y. Zhong, S. Liu, F. Yan, D. Tan, R. Bachelard, C. J. Villas-Boas, A. C. Santos, and D. Yu, Optimal charging of a superconducting quantum battery, *Quantum Science and Technology* **7**, 045018 (2022).
- [24] J.-s. Yan and J. Jing, Charging by quantum measurement, *Phys. Rev. Appl.* **19**, 064069 (2023).
- [25] A. Blais, A. L. Grimsmo, S. M. Girvin, and A. Wallraff,

- Circuit quantum electrodynamics, *Rev. Mod. Phys.* **93**, 025005 (2021).
- [26] H.-Y. Yang, H.-L. Shi, Q.-K. Wan, K. Zhang, X.-H. Wang, and W.-L. Yang, Optimal energy storage in the tavis-cummings quantum battery, *Phys. Rev. A* **109**, 012204 (2024).
- [27] G. Gemme, M. Grossi, D. Ferraro, S. Vallecorsa, and M. Sassetti, Ibm quantum platforms: A quantum battery perspective, *Batteries* **8**, 43 (2022).
- [28] I. Mailllette de Buy Wenniger, S. E. Thomas, M. Maffei, S. C. Wein, M. Pont, N. Belabas, S. Prasad, A. Harouri, A. Lemaître, I. Sagnes, N. Somaschi, A. Auffèves, and P. Senellart, Experimental analysis of energy transfers between a quantum emitter and light fields, *Phys. Rev. Lett.* **131**, 260401 (2023).
- [29] A. Rojo-Francàs, F. Isaule, A. C. Santos, B. Juliá-Díaz, and N. T. Zinner, Stable collective charging of ultracold-atom quantum batteries, *Phys. Rev. A* **110**, 032205 (2024).
- [30] J. F. Barry, J. M. Schloss, E. Bauch, M. J. Turner, C. A. Hart, L. M. Pham, and R. L. Walsworth, Sensitivity optimization for nv-diamond magnetometry, *Rev. Mod. Phys.* **92**, 015004 (2020).
- [31] J. Joshi and T. S. Mahesh, Experimental investigation of a quantum battery using star-topology nmr spin systems, *Phys. Rev. A* **106**, 042601 (2022).
- [32] C. Cruz, M. F. Anka, M. S. Reis, R. Bachelard, and A. C. Santos, Quantum battery based on quantum discord at room temperature, *Quantum Science and Technology* **7**, 025020 (2022).
- [33] H.-P. Breuer, F. Petruccione, *et al.*, *The theory of open quantum systems* (Oxford University, Oxford, 2007).
- [34] F. Pirmoradian and K. Molmer, Aging of a quantum battery, *Phys. Rev. A* **100**, 043833 (2019).
- [35] A. C. Santos, Quantum advantage of two-level batteries in the self-discharging process, *Phys. Rev. E* **103**, 042118 (2021).
- [36] C. A. Downing and M. S. Ukhtary, Hyperbolic enhancement of a quantum battery, *Phys. Rev. A* **109**, 052206 (2024).
- [37] A. C. Santos, B. Çakmak, S. Campbell, and N. T. Zinner, Stable adiabatic quantum batteries, *Phys. Rev. E* **100**, 032107 (2019).
- [38] M. T. Mitchison, J. Goold, and J. Prior, Charging a quantum battery with linear feedback control, *Quantum* **5**, 500 (2021).
- [39] J. Liu, D. Segal, and G. Hanna, Loss-free excitonic quantum battery, *The Journal of Physical Chemistry C* **123**, 18303 (2019).
- [40] K. Xu, H.-G. Li, H.-J. Zhu, and W.-M. Liu, Inhibiting the self-discharging process of quantum batteries in non-markovian noises, *Phys. Rev. E* **109**, 054132 (2024).
- [41] J. Q. Quach and W. J. Munro, Using dark states to charge and stabilize open quantum batteries, *Phys. Rev. Appl.* **14**, 024092 (2020).
- [42] M. Carrega, A. Crescente, D. Ferraro, and M. Sassetti, Dissipative dynamics of an open quantum battery, *New Journal of Physics* **22**, 083085 (2020).
- [43] F. Barra, Dissipative charging of a quantum battery, *Phys. Rev. Lett.* **122**, 210601 (2019).
- [44] A. E. Allahverdyan, R. Balian, and T. M. Nieuwenhuizen, Maximal work extraction from finite quantum systems, *Europhysics Letters* **67**, 565 (2004).
- [45] W. Pusz and S. L. Woronowicz, Passive states and kms states for general quantum systems, *Communications in Mathematical Physics* **58**, 273 (1978).
- [46] Z. Cai, R. Babbush, S. C. Benjamin, S. Endo, W. J. Huggins, Y. Li, J. R. McClean, and T. E. O'Brien, Quantum error mitigation, *Rev. Mod. Phys.* **95**, 045005 (2023).
- [47] J. Etchezarreta Martinez, P. Fuentes, P. M. Crespo, and J. Garcia-Frias, Quantum outage probability for time-varying quantum channels, *Phys. Rev. A* **105**, 012432 (2022).
- [48] O. A. D. Molitor, A. H. A. Malavazi, R. D. Baldijão, A. C. Orthey, I. L. Paiva, and P. R. Dieguez, Quantum switch instabilities with an open control, *Communications Physics* **7**, 373 (2024).
- [49] S. Gherardini, F. Campaioli, F. Caruso, and F. C. Binder, Stabilizing open quantum batteries by sequential measurements, *Phys. Rev. Res.* **2**, 013095 (2020).
- [50] W. M. Itano, D. J. Heinzen, J. J. Bollinger, and D. J. Wineland, Quantum zeno effect, *Phys. Rev. A* **41**, 2295 (1990).
- [51] J. Yi, P. Talkner, and Y. W. Kim, Single-temperature quantum engine without feedback control, *Phys. Rev. E* **96**, 022108 (2017).
- [52] C. Elouard, D. A. Herrera-Martí, M. Clusel, and A. Auffèves, The role of quantum measurement in stochastic thermodynamics, *npj Quant. Inf.* **3**, 1 (2017).
- [53] K. Brandner, M. Bauer, M. T. Schmid, and U. Seifert, Coherence-enhanced efficiency of feedback-driven quantum engines, *New J. of Phys.* **17**, 065006 (2015).
- [54] M. Campisi, J. Pekola, and R. Fazio, Feedback-controlled heat transport in quantum devices: theory and solid-state experimental proposal, *New J. Phys.* **19**, 053027 (2017).
- [55] S. Chand and A. Biswas, Single-ion quantum Otto engine with always-on bath interaction, *Europhys. Lett.* **118**, 60003 (2017).
- [56] S. Chand and A. Biswas, Measurement-induced operation of two-ion quantum heat machines, *Phys. Rev. E* **95**, 032111 (2017).
- [57] M. H. Mohammady and J. Anders, A quantum Szilárd engine without heat from a thermal reservoir, *New J. Phys.* **19**, 113026 (2017).
- [58] C. Elouard, D. Herrera-Martí, B. Huard, and A. Auffèves, Extracting work from quantum measurement in Maxwell's demon engines, *Phys. Rev. Lett.* **118**, 260603 (2017).
- [59] S. Chand and A. Biswas, Critical-point behavior of a measurement-based quantum heat engine, *Phys. Rev. E* **98**, 052147 (2018).
- [60] X. Ding, J. Yi, Y. W. Kim, and P. Talkner, Measurement-driven single temperature engine, *Phys. Rev. E* **98**, 042122 (2018).
- [61] C. Elouard and A. N. Jordan, Efficient quantum measurement engines, *Phys. Rev. Lett.* **120**, 260601 (2018).
- [62] L. Buffoni, A. Solfanelli, P. Verrucchi, A. Cuccoli, and M. Campisi, Quantum measurement cooling, *Phys. Rev. Lett.* **122**, 070603 (2019).
- [63] A. Solfanelli, L. Buffoni, A. Cuccoli, and M. Campisi, Maximal energy extraction via quantum measurement, *J. Stat. Mech.* **2019**, 094003 (2019).
- [64] A. N. Jordan, C. Elouard, and A. Auffèves, Quantum measurement engines and their relevance for quantum interpretations, *Quantum Stud. Math. and Found.* **7**, 203 (2020).

- [65] N. Behzadi, Quantum engine based on general measurements, *J. of Phys. A: Math. and Theo.* **54**, 015304 (2020).
- [66] S. Seah, S. Nimmrichter, and V. Scarani, Maxwell's lesser demon: A quantum engine driven by pointer measurements, *Phys. Rev. Lett.* **124**, 100603 (2020).
- [67] L. Bresque, P. A. Camati, S. Rogers, K. Murch, A. N. Jordan, and A. Auffèves, Two-qubit engine fueled by entanglement and local measurements, *Phys. Rev. Lett.* **126**, 120605 (2021).
- [68] S. Chand, S. Dasgupta, and A. Biswas, Finite-time performance of a single-ion quantum Otto engine, *Phys. Rev. E* **103**, 032144 (2021).
- [69] Z. Lin, S. Su, J. Chen, J. Chen, and J. F. Santos, Suppressing coherence effects in quantum-measurement-based engines, *Phys. Rev. A* **104**, 062210 (2021).
- [70] M. Naghiloo, D. Tan, P. M. Harrington, J. J. Alonso, E. Lutz, A. Romito, and K. W. Murch, Heat and work along individual trajectories of a quantum bit, *Phys. Rev. Lett.* **124**, 110604 (2020).
- [71] M. Naghiloo, J. J. Alonso, A. Romito, E. Lutz, and K. W. Murch, Information gain and loss for a quantum Maxwell's demon, *Phys. Rev. Lett.* **121**, 030604 (2018).
- [72] S. Hernández-Gómez, S. Gherardini, N. Staudenmaier, F. Poggiali, M. Campisi, A. Trombettoni, F. Cataliotti, P. Cappellaro, and N. Fabbri, Autonomous dissipative Maxwell's demon in a diamond spin qutrit, *PRX Quantum* **3**, 020329 (2022).
- [73] P. A. Camati, J. P. S. Peterson, T. B. Batalhão, K. Micadei, A. M. Souza, R. S. Sarthour, I. S. Oliveira, and R. M. Serra, Experimental rectification of entropy production by Maxwell's demon in a quantum system, *Phys. Rev. Lett.* **117**, 240502 (2016).
- [74] M. F. Anka, T. R. de Oliveira, and D. Jonathan, Measurement-based quantum heat engine in a multi-level system, *Phys. Rev. E* **104**, 054128 (2021).
- [75] M. S. Alam and B. P. Venkatesh, Two-stroke quantum measurement heat engine, *arXiv:2201.06303* (2022).
- [76] S. K. Manikandan, C. Elouard, K. W. Murch, A. Auffèves, and A. N. Jordan, Efficiently fueling a quantum engine with incompatible measurements, *Phys. Rev. E* **105**, 044137 (2022).
- [77] N. M. Myers, O. Abah, and S. Deffner, Quantum thermodynamic devices: From theoretical proposals to experimental reality, *AVS Quantum Sci.* **4**, 027101 (2022).
- [78] V. Lisboa, P. Dieguez, J. Guimarães, J. Santos, and R. Serra, Experimental investigation of a quantum heat engine powered by generalized measurements, *Phys. Rev. A* **106**, 022436 (2022).
- [79] P. R. Dieguez, V. F. Lisboa, and R. M. Serra, Thermal devices powered by generalized measurements with indefinite causal order, *Phys. Rev. A* **107**, 012423 (2023).
- [80] O. Oreshkov and T. A. Brun, Weak measurements are universal, *Physical review letters* **95**, 110409 (2005).
- [81] P. R. Dieguez and R. M. Angelo, Information-reality complementarity: The role of measurements and quantum reference frames, *Phys. Rev. A* **97**, 022107 (2018).
- [82] Y. Pan, J. Zhang, E. Cohen, C.-w. Wu, P.-X. Chen, and N. Davidson, Weak-to-strong transition of quantum measurement in a trapped-ion system, *Nature Physics* **16**, 1206 (2020).
- [83] L. Mancino, M. Sbroscia, E. Roccia, I. Gianani, F. Somma, P. Mataloni, M. Paternostro, and M. Barbieri, The entropic cost of quantum generalized measurements, *npj Quantum Information* **4**, 1 (2018).
- [84] J. J. Alonso, E. Lutz, and A. Romito, Thermodynamics of weakly measured quantum systems, *Physical review letters* **116**, 080403 (2016).
- [85] C. Vieira, J. de Oliveira, J. Santos, P. Dieguez, and R. Serra, Exploring quantum thermodynamics with nmr, *Journal of Magnetic Resonance Open* **16-17**, 100105 (2023).
- [86] M. A. Balkanlu, E. Faizi, and B. Ahansaz, Selective weak measurement reveals super-ergotropy, *Results in Physics* **57**, 107308 (2024).
- [87] G. Francica, J. Goold, F. Plastina, and M. Paternostro, Daemonic ergotropy: enhanced work extraction from quantum correlations, *npj Quantum Information* **3**, 12 (2017).
- [88] Y.-S. Kim, J.-C. Lee, O. Kwon, and Y.-H. Kim, Protecting entanglement from decoherence using weak measurement and quantum measurement reversal, *Nature Physics* **8**, 117 (2012).
- [89] X. Xiao and Y.-L. Li, Protecting qutrit-qutrit entanglement by weak measurement and reversal, *The European Physical Journal D* **67**, 204 (2013).
- [90] W.-J. Zou, Y.-H. Li, S.-C. Wang, Y. Cao, J.-G. Ren, J. Yin, C.-Z. Peng, X.-B. Wang, and J.-W. Pan, Protecting entanglement from finite-temperature thermal noise via weak measurement and quantum measurement reversal, *Phys. Rev. A* **95**, 042342 (2017).
- [91] A. N. Korotkov and K. Keane, Decoherence suppression by quantum measurement reversal, *Phys. Rev. A* **81**, 040103 (2010).
- [92] S.-C. Wang, Z.-W. Yu, W.-J. Zou, and X.-B. Wang, Protecting quantum states from decoherence of finite temperature using weak measurement, *Phys. Rev. A* **89**, 022318 (2014).
- [93] K. Wang, X. Zhao, and T. Yu, Environment-assisted quantum state restoration via weak measurements, *Phys. Rev. A* **89**, 042320 (2014).
- [94] J.-C. Lee, Y.-C. Jeong, Y.-S. Kim, and Y.-H. Kim, Experimental demonstration of decoherence suppression via quantum measurement reversal, *Opt. Express* **19**, 16309 (2011).
- [95] J. Lalita and S. Banerjee, Protecting quantum correlations of negative quantum states using weak measurement under non-markovian noise, *Physica Scripta* **99**, 035116 (2024).
- [96] A. Streltsov, G. Adesso, and M. B. Plenio, Colloquium: Quantum coherence as a resource, *Rev. Mod. Phys.* **89**, 041003 (2017).
- [97] G. Francica, F. C. Binder, G. Guarnieri, M. T. Mitchison, J. Goold, and F. Plastina, Quantum coherence and ergotropy, *Phys. Rev. Lett.* **125**, 180603 (2020).
- [98] T. Guha, S. Roy, K. Simonov, and Z. Zimborás, Activation of thermal states by quantum switch-driven thermalization and its limits, *arXiv:2208.04034* (2022).
- [99] Z. Niu, Y. Wu, Y. Wang, X. Rong, and J. Du, Experimental investigation of coherent ergotropy in a single spin system, *arXiv:2409.06249* (2024).
- [100] S. Vinjanampathy and J. Anders, Quantum thermodynamics, *Contemporary Physics* **57**, 545 (2016).
- [101] T. Werlang, M. A. Marchiori, M. F. Cornelio, and D. Valente, Optimal rectification in the ultrastrong coupling regime, *Phys. Rev. E* **89**, 062109 (2014).
- [102] M. Łobejko, P. Mazurek, and M. Horodecki, Thermodynamics of Minimal Coupling Quantum Heat Engines,

- [Quantum](#) **4**, 375 (2020).
- [103] S. Bhattacharjee and A. Dutta, Quantum thermal machines and batteries, [The European Physical Journal B](#) **94**, 239 (2021).
- [104] A. H. A. Malavazi, B. Ahmadi, P. Mazurek, and A. Mandarino, Detuning effects for heat-current control in quantum thermal devices, [Phys. Rev. E](#) **109**, 064146 (2024).
- [105] H. Ollivier and W. H. Zurek, Quantum discord: A measure of the quantumness of correlations, [Phys. Rev. Lett.](#) **88**, 017901 (2001).
- [106] P. R. Dieguez and R. M. Angelo, Weak quantum discord, [Quantum Inf. Process.](#) **17**, 1 (2018).